Validation of a CFD Model of a Single Stage Centrifugal Compressor by Local Flow Parameters

Sergey Bogdanets
Ural Federal University named after the first President of Russia B.N. Yeltsin
Yekaterinburg, Russia
bogdanec1996@rambler.ru

Vitaly Blinov
Ural Federal University named after the first President of Russia B.N. Yeltsin
Yekaterinburg, Russia
vithomukyn@mail.ru

Vyacheslav Sedunin
Ural Federal University named after the first President of Russia B.N. Yeltsin
Yekaterinburg, Russia
lerr@bk.ru

Oleg Komarov
Ural Federal University named after the first President of Russia B.N. Yeltsin
Yekaterinburg, Russia
ov_komarov@mail.ru

Alexander Skorohodov
Ural Federal University named after the first President of Russia B.N. Yeltsin
Yekaterinburg, Russia
skorohodov@gmail.com

Abstract

In this article, CFD model validation results of a single-stage centrifugal compressor is presented. Based on a local parameters comparison for static pressure, meridional velocity and flow angles in absolute motion, the paper describes aerodynamic flow features in the flow path, both those adequately predicted and those that not.

1 Introduction

This work is devoted to the verification of a computational model of a centrifugal compressor with an axial inlet impeller and a vaneless diffuser. These types of stages become necessary when the rotational speed of the drives is constantly increasing [1]. The advantage of axial inlet impeller is in greater total head compared to simple radial designs with identical circumferential speeds [2]. For the design of centrifugal compressors with a high efficiency, it is necessary to consider the three-dimensional physical effects occurring in its passage. At present, the application of the methods of computational fluid dynamic (CFD) has become an integral part of various researches, and requirements to accuracy of such results are also increasing. Paper [3] summarizes results of numerous fluid dynamics studies in centrifugal compressors.

The flow in the centrifugal wheel is described by the jet-wake model, which Dean first described in [4]. Later, this model was experimentally confirmed by Eckardt [5]. The appearance and development of a wake zone can be highly dependent on the tip flow above unshrouded impeller. Many numerical investigations determine and establish jet-wake flow model [6,7]. In an investigation [8] basic mechanism leading to the formation of the jet/wake flow structure in centrifugal machines is given. Numerous numerical simulations were made, on basic of which vortexes, vortices and leakage flows were described and studied.

The compressor of interest is shown in Fig. 1 and it consists of an unshrouded impeller and a vaneless diffuser. Experimental data for comparison was taken from [5].

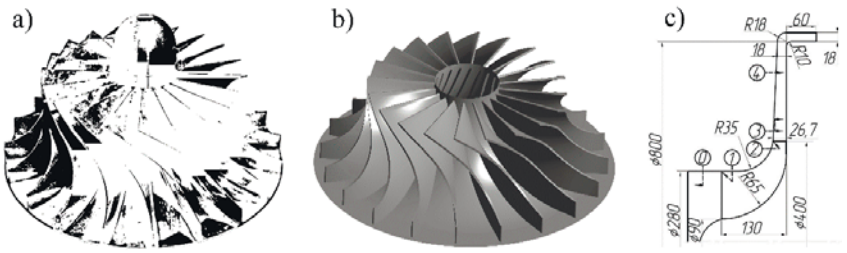

Figure 1. Impeller of centrifugal compressor a) - a photo of Eckardt impeller [5], b) - 3D model, c) Main dimensions and measuring points positions, measurements in mm

2 Statement research

The experimental results, obtained by D. Eckardt et.al. in [4] were used for verification. An in-house code was used to create a 3D model of the compressor flow path (Figure 1a), geometry data from the report, partially shown on Figure 1b.

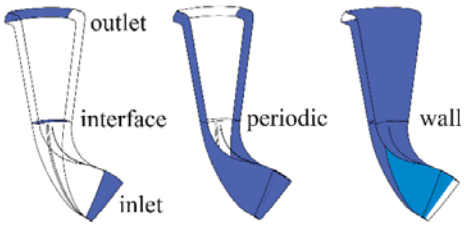

Figure 2. Boundary conditions of numerical model

Figure 2 shows the types of boundary conditions at surfaces of domain. It was as: a total pressure of 101325 Pa and total temperature of 288K at the inlet and mass flow at the diffuser outlet. These boundary condition were chosen in order to have stable convergence above the design operating point. The radial tip with relative magnitude of about 0.5% to 2.6% was simulated by the GGI interface. Periodic boundary conditions were applied at the side faces of the model. To study the mixing of the jet-wake in the diffuser, a frozen rotor interface was set between rotating and stationary domains. The turbulence model k-ε allows to reduce computational cost due to the coarser grid. Fluid – air ideal gas. Mesh size for both domains is 540,000 elements. Convergence criteria: below than 10^{-6} and stabilized value of the compressor efficiency.

3 Processing results

3.1 Validation by mass-averaged parameters

Computed performance of the compressor is plotted on Figure. 3a. It shows that the numerical model predicts less loading coefficient and earlier stability loss. When the shaft speed is low, the speed lines better match with the experimental ones, but as the rpm goes up, computed lines appear to have counterclockwise turn compared to the experiment.

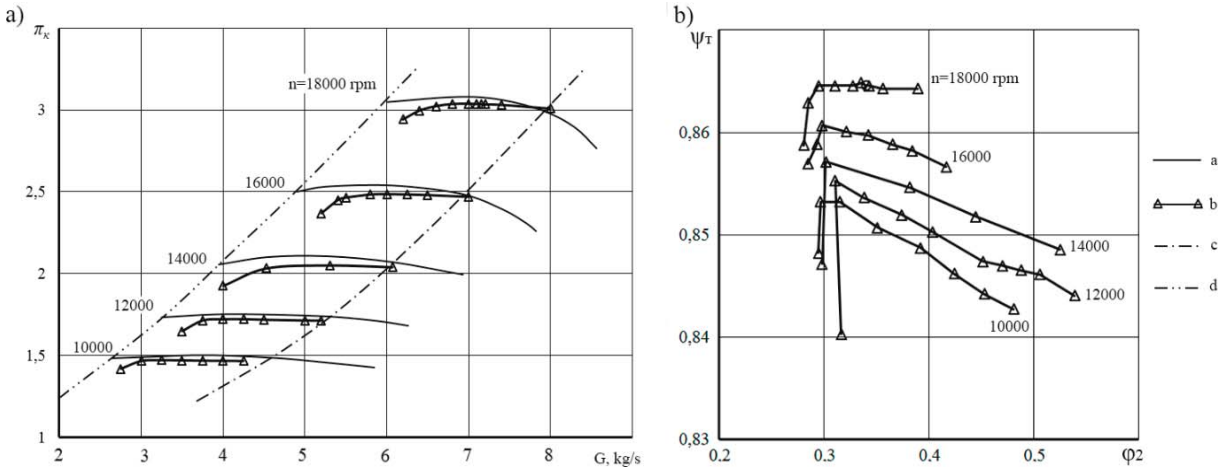

Figure 3. a) - Performance characteristic of a compressor pressure ratio versus mass flow and b) - Performance characteristic of a compressor loading coefficient versus flow coefficient. 1– lines of constant rotational speed in experiment, 2 – lines of constant rotational speed in numerical simulation, 3 – throttle ring curve, 4 – surge limit

Figure 3b shows that the pressure ratio increases linearly with decreasing flow, up to a certain value, which determines the onset of stall. Lines with lower rpm have bigger slope. This is explained by large change in the deviation angle in the speed lines at a higher rate. At the nominal speed line, the deviation angle increases by 4 degrees, between speed lines of 0.67 and 0.56 by 2 degrees. Analysis of Mach number distribution (Figure 4) revealed that a sharp drop in pressure ratio is due to the formation of vortices behind the trailing edge and from overflow through the radial clearance at the inlet. This vortex causes a decrease in the flow rate at the shroud, which increases the angle of attack at the shroud and a small separation on the back of the blade. Also, as the flow rate decreases, the losses in the diffuser increase non-linearly (Figure 5).

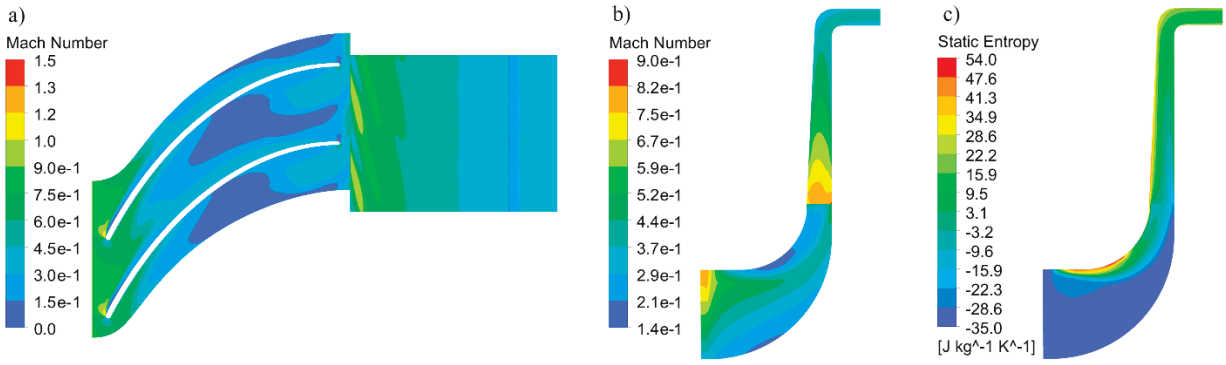

Figure 4. a) - Mach number contour at the surface span=0.95 and b) - at the meridional section. c) - Static entropy contour at the meridional section. Stall mode at nominal rotating speed.

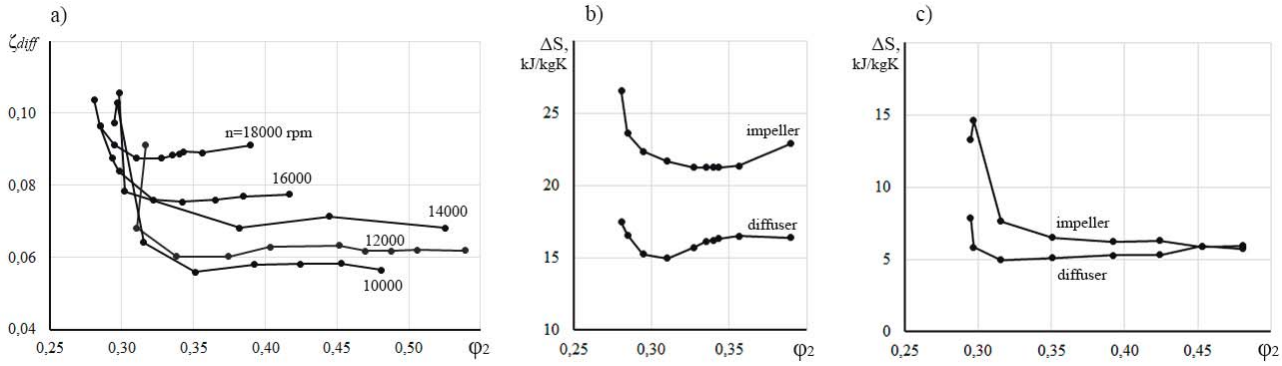

Figure 5. a) - Total pressure loss coefficient versus flowing coefficient. b) - The entropy gain (2) in the impeller and in the diffuser versus flowing coefficient at the nominal rotating speed c) - at the 0.56 nominal rotating speed

Figure 5 shows that the dependence of the total pressure loss coefficient in the diffuser, which is calculated based on expression (1) for identical flow coefficient at all speed lines. At the operating points away from surge, losses in the diffuser are almost independent of the mass flow. With lowering flow there is even a slight decrease in losses, but after a certain flow a rapid loss gain happens.

$$\zeta_{diff} = \frac{P_{4t} - P_{2t}}{P_{2t} - P_{1t}} \tag{1}$$

Where ζ_{diff} is the total pressure loss coefficient into diffuser, P_{4t}, P_{2t}, P_{1t} are total pressure at diffuser outlet, impeller outlet and impeller inlet respectively.

From the analysis of Figures 3b and 5a it can be seen that the shift of the performance characteristic (Fig. 3a) is caused by a change in the losses in the diffuser. This can also explain almost horizontal slope of the speed lines as for $\psi_T=f(\varphi_2)$. The high speed line has a horizontal dependence $\psi_T=f(\varphi_2)$, and the worst qualitative coincidence with the experimental speed line.

Total pressure ratio of the impeller (section 0-2) in computation is less, static pressure ratio is greater. The difference between the total pressure ratio between the 0-2 and 0-4 sections in the computation is less, which indicates a lower total pressure loss in the diffuser compared to the experiment. Total pressure ratio of the stage is lower than in the experiment, because of the lower total pressure ratio of the impeller.

Losses in the impeller and diffuser are determined as entropy gain ΔS. The entropy gain in the impeller and in the vaneless diffuser versus the mass flow is shown in Fig. 5b,5c and is calculated based on expressions (2). This dependence has character of changing like the total pressure loss coefficient.

$$\Delta S = c_p * \ln\left(\frac{T_{2t}}{T_{1t}}\right) - R * \ln\left(\frac{P_{2t}}{P_{1t}}\right) \tag{1}$$

Where c_p is specific heat at constant pressure, R is gas constant, T_{2t}, T_{1t} are total temperature at impeller outlet and impeller inlet respectively.

The main loss source in the impeller is expected to be due to the tip leakage flows (Figure 4c). These losses are less for lower rotor speeds [3]. The error in verification decreases with decreasing rotational speed, which may be caused by a more accurate prediction of the vortex at the shroud.

3.2 Validation by local flow parameters at the design speed

The following comparison is presented for the design operating point. Based on his results Eckardt presents a flow pattern in the radial part of the blade channel, which is shown in Figure 6A. Figure 6B shows for comparison similar scheme of the velocity vector pitch wise components on the circumferential surface *x/s=0.87* based on computation. It

can be seen that in the numerical simulation the vortex occupies a large area and is shifted to the pressure side. This vortex must form a "wake", which affects the distribution of parameters across the section.

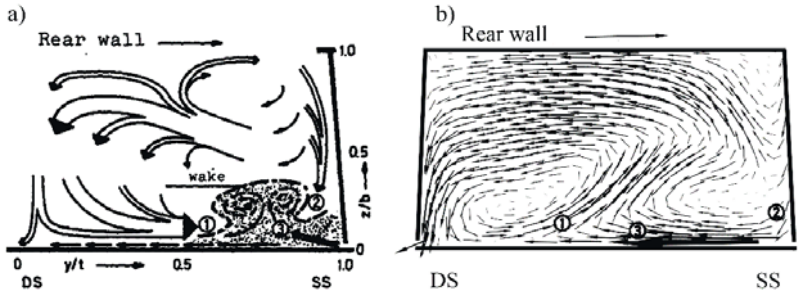

Figure 6. Secondary flow pattern in the radial part of the impeller blade channel *x*/s=0.87
a) - Eckardt [1]; b) - numerical simulation

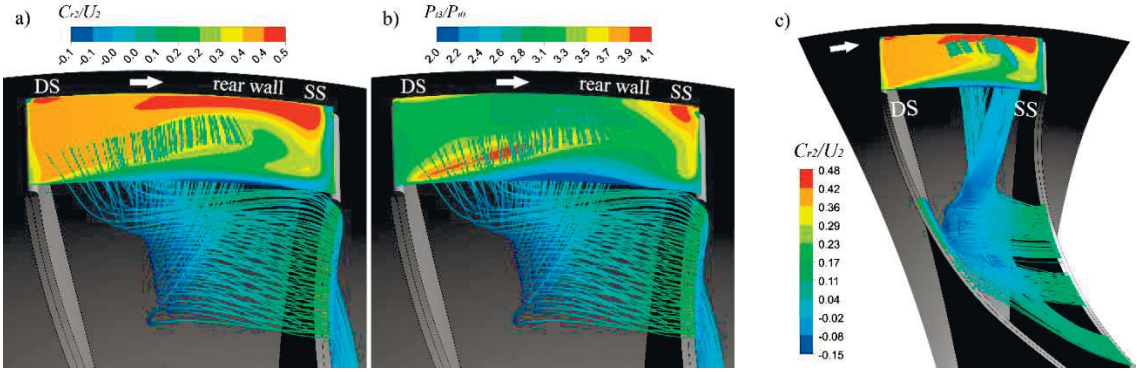

Figure 7. Streamlines from the radial tip a) - contour C_r/U_2; b) - contour P_{t3}/P_{t0};
c) - streamlines from the middle of blade C_r/U_2 R/R_2=1.017

The image of the streamlines together with the contour of C_r/U_2 and P_{t3}/P_{t0} (Figure 7) makes it possible to determine the causes of the zones with low parameters near the front wall and suction side (in the pictures this area is bottom right). These zones are due to tip flow. The vortex appearing at the tip near outlet defines the boundaries of these zones (Figure 7A).

3.3 Validation by local flow parameters at the rotational speed of 0.78

Figure 8 shows the sections in which the data sets were measured for plotted contours of velocity and flow angle.

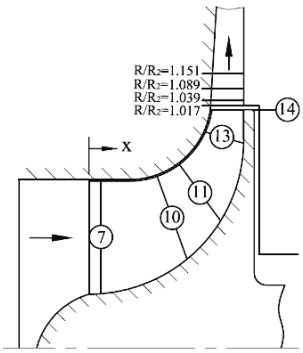

impeller	x/Sm	7	0,08
		10	0,43
		11	0,59
		13	0,87
		14	1,01
vaneless diffuser	R/R2	1	1,017
		2	1,039
		3	1,089
		4	1,151

Figure 8. Location of the measuring sections

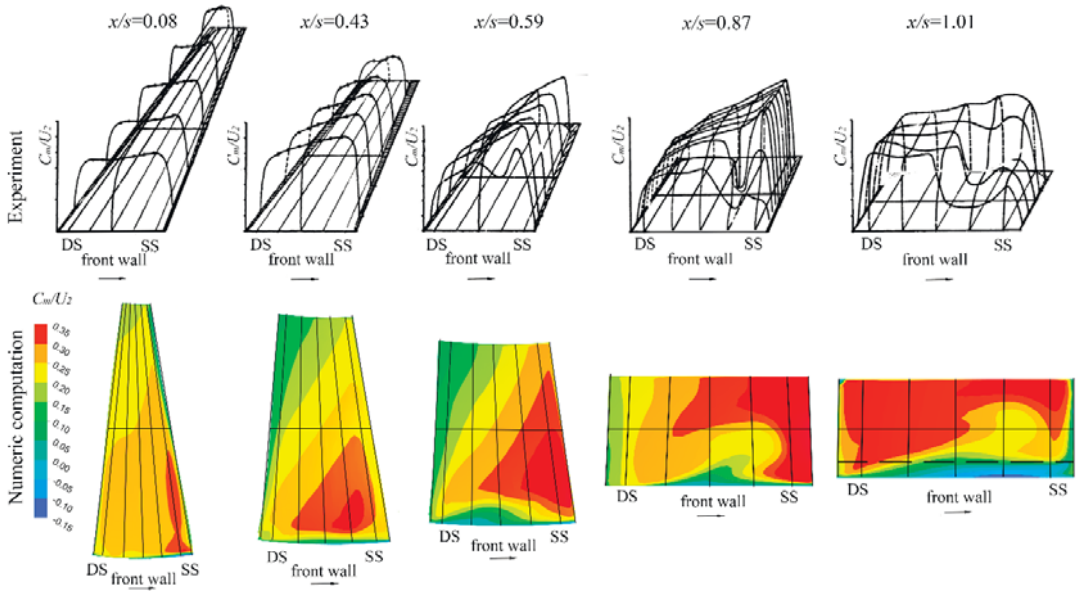

Figure 9. Contours C_m/U_2 at the various sections

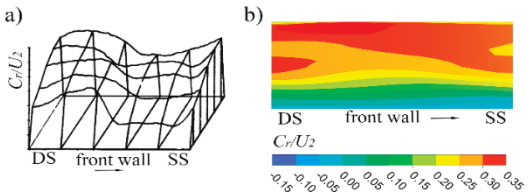

Figure 10. Contour C_m/U_2 at the section R/R_2=1.151. a) - experiment; b) - numerical simulation

Figures 9 and 10 show contours of meridional velocity to blade velocity ratio after impeller C_m/U_2 at different sections (Figure 8).

In section 7 the shape of the meridional velocity distribution coincides with experiment. A similar qualitative agreement was found in section 10. This section is the last for the axial part of the impeller. The core of the stream is at the suction side close to casing, the stream has not yet been divided into jet and wake zones.

Section 11 is diagonal, in which the core flow has not yet shifted to the hub surface, but a vortex has already appeared from the tip leakage. Therefore a starting position of this vortex is predicted more or less correctly.

Section 13 is located on the radial section of the impeller and there is a developed tip vortex. The core has shifted to the suction side, both in experiment and in computation. In this section, the flow is described by a jet-wake model and there are differences between computation and experiment. The core in the computation is stretched over the suction side because the tip vortex stays at the middle of the channel.

The flow core in section 14 is shifted to the rear wall, which is caused by a flow turning from axial to radial direction. Considering the thickness of the radial tip and nonzero dimensions of a pitot tube in the experiment, one can draw an approximate line behind which the experimental data was not obtained. Then, comparing the contours, it can be seen that the jet-wake zones in the computation and in the experiment are qualitative agreed. The flow core at the computation extends over a larger area, being also in the middle of the channel. Section 14 is located after the trailing edge.

The contour in the section of diffuser R/R_2 = 1.151 shows increasing of the vortex size and mixing of the one with the flow in the tangential direction, which does not happen in the experiment.

In the computation, the boundary layer is very thin as compared with the experiment. Therefore, area of the flow core in computation is bigger which cause a change in the mass averaged velocity diagram.

In computation, the vortex from the radial tip proceeds to the pressure side direction, although in the experiment the vortex moves towards the hub direction along the suction side right after exiting the tip.

Figure 11 shows distributions of the flow exit angle in absolute frame - α_2. The representation of the distributions in the form of constant value lines allows for a quantitative comparison. A decreased angle α_2 indicates the increased radial absolute velocity C_r, when other velocity components remain equal. Decreased C_{2r} along the wall indicates that the causes a slowing of the flow. Therefore, the contour α_2 in the section $R/R_2=1,017$ shows that in the computation the thickness of the boundary layer at the hub is smaller than one in the experiment.

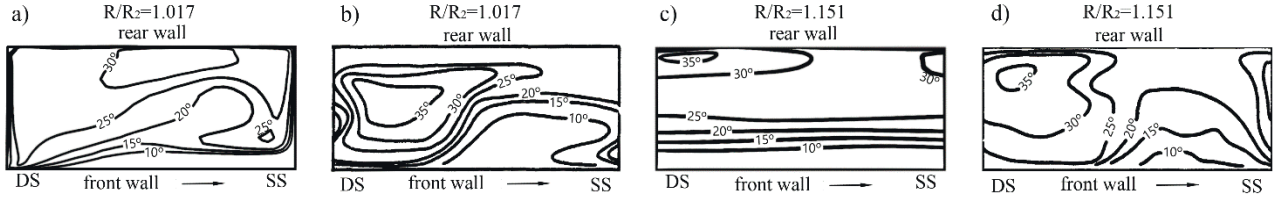

Figure 11. Contours of the flow exit angle in the absolute frame α_2 a), c)- numerical simulation; b), d)- experiment

The contour of α_2 in the section of $R/R_2=1,017$ allows to estimate quantitative difference. The zone of angles by 25º-20º in the computation and the experiment beat a qualitative similarity. An absence of a developed boundary layer near the hub is the difference. The presence of this layer would allow this zone (angles by 25º-20º) to expand like in the experiment and, perhaps, would shift the flow core (30-35º) toward the pressure side. In computation compared to the experiment, there is no zone of angles > 35º. Therefore, area of the flow core in the computation is larger due to negligibly small boundary layer. The zone of angles below 10 degrees is defined by a vortex and has the biggest difference compared to the experiment: the gradient is higher in the computation.

In the section $R/R_2=1,151$, the zone of angles more than> 35 º is appeared. In the computation there is an intense tangential mixing of the zones by 5º-25º, compared to the experiment. The numerical model predicts the undeveloped boundary layer near the hub. The mixing of the flow behind the impeller is faster than in the experiment.

4 Conclusion

It was found that for the design operating point the difference in the integral characteristics between the numerical simulation and the experiment is less than 1.2%. Main conclusions are drawn from comparison of local flow parameters at different sections at different operating conditions:

1. It was shown that the vortex is formed at the same place where Dean determined in his work [4]. But the numerical simulation predicts the vortex being stretched along the front wall. This vortex doesn't move into the flow path as it was seen in the experiment.

2. Underestimation of the boundary layer on solid surfaces affect the flow pattern in the numerical simulation. This causes increased diffusivity and earlier onset of stall. Therefore, the surge limit in the computation is shifted to the right due to earlier prediction of flow separation at the angle between the shroud and the trailing edge. Increased diffusivity in the computation provides more effective deceleration of the flow in the impeller. This leads to a less density of the working fluid. Provided that the air flow is the same, computed exit speed is lower, which cause less hydraulic losses. This explains greater efficiency in the computation.

3. In the numerical simulation zones of jet and wake mix earlier at the diffuser, therefore pressure losses in the diffuser are lower.

4. The slope shift of the computed characteristics compared to the experimental ones was observed especially with increasing rotational speed. Improving convergence of computed and experimental speed lines at lower speeds is a consequence of better prediction of the deviation angle and losses from the dissipation of the radial tip vortex. Also, the supersonic flow at the casing at higher speeds adds complexity to the model.

5.The numerical model is reasonably good at prediction of overall performance and flow features occurring in the flow path at the design operating point. Further away from the nominal, accumulation of numerical errors leads to bigger errors. These errors must be investigated to improve the quality of numerical simulations.

References

1. Galerkin YU.B. Voprosy proektirovaniya protochnoj chasti centrobezhnyh kompressorov prirodnogo gaza // Kompressornaya tekhnika i pnevmatika v XXI veke: XIII Mezhdunarodnaya nauchno-tekhnicheskaya konferenciya po kompressorostroeniyu. Sumy: SumGU, 2004. p. 166-188.
2. Revzin B.S. Gazoperekachivayushchie agregaty s gazoturbinnym privodom. 2-e izd., Ekaterinburg: GOU UGTU-UPI, 2002. 269 p.
3. Kumpsty N.A. Compressor aerodynamic 2000.- 688p
4. Dean R.C. On the unresolved fluid dynamics of the centrifugal compressor. ASME ch 1, 1971
5. Eckardt D. Investigation of the jet-wake flow of a highly-loaded centrifugal compressor impeller Doctoral Dissertation, Rhein Westfael Technical School, Aachen, West Germany, (1977), PP. 1-227
6. Dachdanai Boonchauy, Kittipass Wasinarom, Monthol Chamsab and Jaruwat Charoensuk Computational investigation of quantitative entropy generation in centrifugal compressors with different exit beta angle The Second TSME International Conference on Mechanical Engineering 2011
7. Zheng Qun, Liu Shun-long Topological analysis of the formation of Jet-Wake flow pattern in centrifugal impeller channel Journal of Marine Science and Application 2004
8. Shun Kang, Charles Hirsch. Numerical simulation and theoretical analysis of the 3d viscous flow in centrifugal impellers Task Quarterly 2001